Materials and Design 43 (2013) 66–73

Contents lists available at SciVerse ScienceDirect

Materials and Design

journal homepage: www.elsevier.com/locate/matdes

Effects of heat treatments on the microstructure and mechanical properties of Rene 80

Caixiong Yang [a], Yulai Xu [a], Heng Nie [a], Xueshan Xiao [a,*], Guoqing Jia [b], Zhi Shen [b]

[a] Laboratory for Microstructures, Institute of Materials, Shanghai University, Shanghai 200072, China
[b] Shanghai Electric Power Generation Equipment Co., Ltd. Turbine Works, Shanghai 200240, China

ARTICLE INFO

Article history:
Received 7 May 2012
Accepted 17 June 2012
Available online 4 July 2012

Keywords:
Non-ferrous alloy
Heat treatment
Mechanical properties
Microstructure

ABSTRACT

Effects of heat treatments on room temperature mechanical properties and stress-rupture properties of Rene 80 have been investigated. The microstructures were analyzed by optical microscope and scanning electron microscope after each step of heat treatments. With the decrease of aging temperature, the average size of γ′ phase decreases, but the volume fraction of γ′ phase increases. The lower aging temperature suppresses the growing of the coarse γ′ particles, but facilitates the growth of the fine γ′ particles. After the optimum heat treatment, the ultimate tensile strength and yield strength are respectively higher than 1040 MPa and 950 MPa, the stress-rupture life at 871 °C/310 MPa is higher than 170 h with excellent ductility. The improved tensile strength and stress-rupture life are primarily due to the increased volume fraction of γ′ phase. The borides precipitate at grain boundaries at about 913 °C. The primary MC is found to decompose into M_6C at about 873 °C and $M_{23}C_6$ at 840–873 °C at grain boundaries. The precipitate of the carbides may partly contribute to the improved mechanical properties.

1. Introduction

Nickel-based superalloys are important materials for aerospace and power plant applications where high temperature strength and creep resistance are critical [1]. The cast nickel-based superalloy Rene 80 is commonly used to manufacture the first and second stage turbine blades in modern jet engines due to its excellent combination of high stress-rupture strength, thermal fatigue and hot corrosion resistance [2–4]. Rene 80 is generally used at temperature of 760–982 °C and the microstructure of Rene 80 consists of γ matrix, γ′ phase precipitates in the γ matrix and the carbides. The γ′ phase which precipitates during heat treatment is derived from ordered face-centered cubic (FCC) crystal structure ($L1_2$) with corners of the unit cell occupied by Al or Ti atoms and face centers occupied by Ni atoms [5]. The most significant contribution to the strength of nickel-based superalloy is the coherent precipitate of the γ′ phase [6,7]. Much of the high temperature strength and microstructural stability of nickel-based superalloy rely on the formation of the γ′ phase and its volume fraction, size and distribution [8]. Increasing of the γ′ volume fraction enhances the γ′ solvus temperature, which enables an alloy to retain strength at higher service temperatures [9]. The presence of up to 70% of the ordered γ′ phase provides significant strengthening in nickel based superalloys [10].

Carbides also play a complex role in nickel-based superalloys and the high temperature properties can be improved in many circumstances if the proper proportion of carbon element is present [11]. Coarse primary carbide of type MC is rich in Ti, Mo and W elements, M_6C carbide is rich in Ni, Co, Mo and Cr elements, $M_{23}C_6$ carbide is rich in Cr element at the grain boundaries [12]. The carbides prefer to precipitate at the grain boundaries, which has a beneficial effect on the high temperature strength via the inhibition of grain boundary sliding. However, the precipitate of carbides can also facilitate crack initiation and propagation sometimes and the function of carbides in nickel-based superalloys depends mainly on their geometry and distribution [13]. The script-like and elongated carbides can precipitate when the carbon content is too high in the superalloy, which can impair the mechanical properties. Moreover, the script-like and elongated carbides may also cause the fracture modes of superalloy change from the typical intergranular mode to transgranular and intergranular mixed modes [14]. Small M_3B_2 particle with average size of 500 nm rich in Mo, W and Cr is found at the grain boundaries in Rene 80, and the increasing fraction of grain boundaries with densely spaced borides can increase the cracking susceptibility [15].

The most common techniques to optimize the properties of most γ′ strengthened superalloys are the addition of various alloying elements and the use of suitable heat treatments to control the size and morphology of the γ′ phase. A number of investigations have been carried out on the mechanical properties and the deformation mechanism of Rene 80 [16–18]. However, the effect of different aging treatments on the stress-rupture properties has

* Corresponding author. Tel./fax: +86 21 56331484.
E-mail address: xsxiao@mail.shu.edu.cn (X. Xiao).

0261-3069/$ - see front matter © 2012 Elsevier Ltd. All rights reserved.
http://dx.doi.org/10.1016/j.matdes.2012.06.039

hardly been reported. In this paper, microstructures after each step of heat treatments were analyzed to have a deep understanding of its evolution. The room temperature mechanical properties and stress-rupture properties were investigated after different aging treatments, and the strengthening mechanism was correlated with the microstructures.

2. Experimental details

The chemical compositions of the cast nickel-based superalloy Rene 80 are Ni–14.6Cr–3.97W–4.50Mo–8.69Co–3.01Al–4.94Ti–0.17C (wt.%). The alloys were melted in a 50 kW induction furnace in a vacuum atmosphere. In order to eliminate the chemical segregation and the γ–γ′ eutectic in the cast ingot, solution heat treatment was carried out at 1204 °C/2 h AC (air cooling) + 1093 °C/4 h AC + 1054 °C/4 h AC. Then the alloys were aged at 913 °C, 873 °C and 840 °C for 16 h, respectively.

After fully heat treated, room temperature tensile tests were performed on round bar samples with a gauge length of 25 mm and diameter of 5 mm according to the National Standard of the PR China, GB/T228-2002 [19], and a strain rate of $1 \times 10^{-3}\ s^{-1}$ was used in the tests to determine the mechanical properties including the ultimate tensile strength (σ_b), yield strength (σ_s) and total elongation (ε). Stress-rupture tests were carried out under the condition of the applied stress of 310 MPa at 871 °C. The specimens for the stress-rupture tests were prepared according to the National Standard of the PR China, GB/T2039-1997 [20]. The samples were crept up to fracture, at least three samples were prepared for the stress-rupture tests and the average value was taken as the stress-rupture life. The schematic diagrams of the specimens are shown in Fig. 1.

The microstructures of the samples after each step of heat treatments were analyzed by KEYENCE VH-Z100 optical microscope (OM) and HITACHI SU-1510 scanning electron microscope (SEM) equipped with energy dispersive spectroscopy (EDS). The metallographic samples for OM and SEM were prepared by grinding using SiC abrasive papers from No. 200 up to No. 2000, polishing using 1.0 μm diamond abrasive, and then electro-etching in a solution with 10 ml HNO_3, 30 ml HCl and 30 ml H_2O at 10 V for 3 s.

3. Results and discussion

Room temperature tensile tests were performed on the alloys after aging treatment at 913 °C, 873 °C and 840 °C for 16 h, respectively. The variations of σ_b, σ_s and ε of the alloys at room temperature are shown in Table 1, which indicates that the alloys after aging at lower temperatures show better mechanical properties. The σ_b and σ_s are respectively about 940 MPa and 795 MPa for the alloys after aging at 913 °C. When the aging temperature decreases to 873 °C, the σ_b and σ_s respectively increase by about 5.9% and 3.1% compare with those after aging at 913 °C. After aging at 840 °C, the σ_b and σ_s further increase to about 1040 MPa and 950 MPa, respectively. What is more, the elongation ε slightly increases with the decrease of aging temperature. Stress-rupture tests were carried out under the condition of the applied stress of 310 MPa at 871 °C. The stress-rupture life increases from about 120 h–174 h when the aging temperature decreases from 913 °C to 840 °C (Table 1). Besides, both the high temperature elongation and reduction in area are improved with the decrease of aging temperature.

The OM and SEM micrographs of the cast Rene 80 are shown in Fig. 2. The microstructure of the cast alloy consists of the dendrite segregation patterns (Fig. 2a). Due to the segregation of heavy elements such as W and Mo at the core of dendrite, while Al and Ti elements enrich in the inter-dendrite region, the electro-chemically etching made the dendrite region bright and the inter-dendrite region gray (Fig. 2b). Fig. 2c shows the morphology of γ–γ′ eutectic in the inter-dendrite region and the average size of the γ′ phase in the inter-dendrite region is slightly larger than that in the dendrite region. The blocky carbide is also identified in the inter-dendrite region. The corresponding SEM-EDS shows that the carbide is rich in Ti, W and Mo elements (Fig. 2d), which can be inferred to be MC carbide according to the previous research [12].

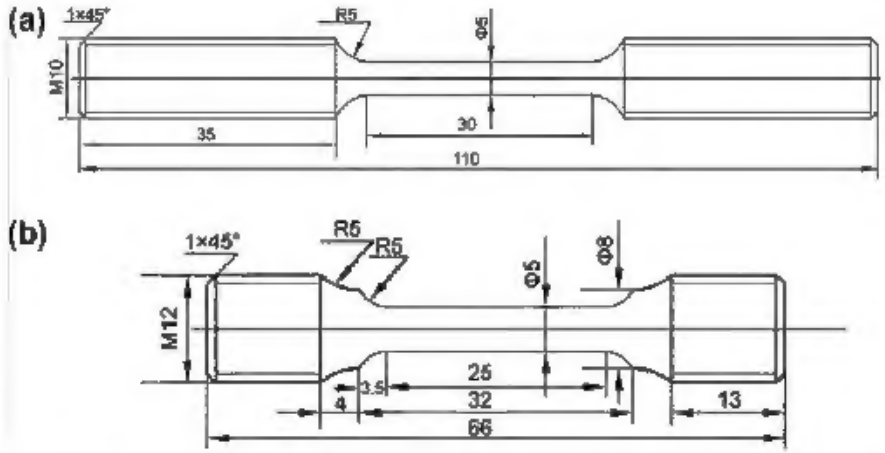

Fig. 1. Schematic diagrams of the (a) room temperature tensile test specimens and (b) stress-rupture test specimens (all dimensions are in millimeters).

Table 1
The variations of σ_b, σ_s and δ at room temperature, and the stress-rupture life, ε and ψ at 871 °C/310 MPa.

Aging temperature (°C)	σ_b/MPa	σ_s/MPa	δ/%	Stress-rupture life/h	ε/%	ψ/%
913	940	795	2.09	120	4.0	5.0
873	995	820	2.87	155	5.5	6.0
840	1040	950	3.18	174	6.5	6.7

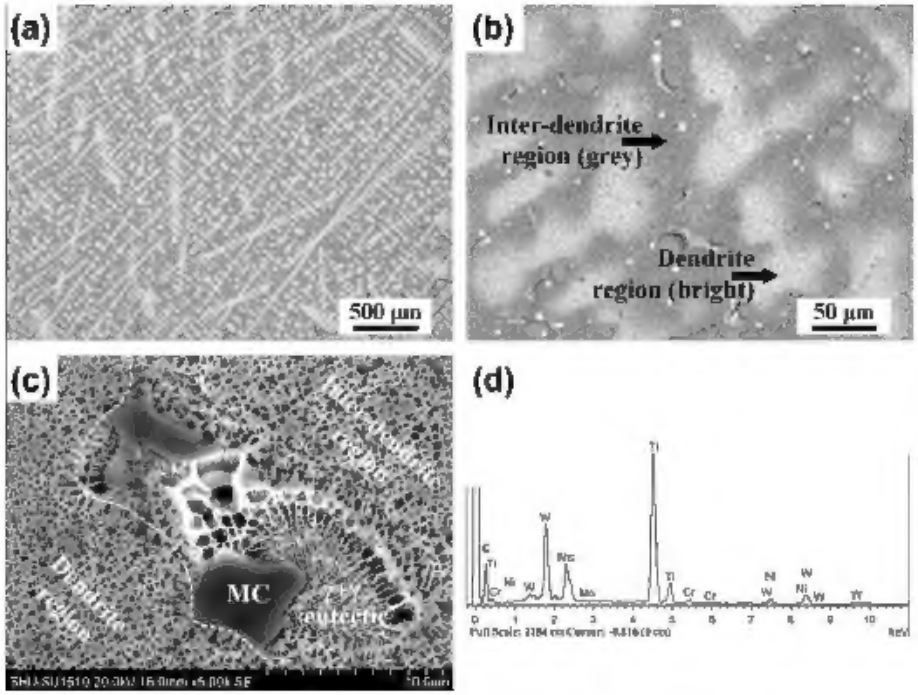

Fig. 2. Microstructure of Rene 80, (a) the optical micrograph shows the dendritic patterns of the casting, (b) enlarged dendritic patterns show the dendrite and inter-dendrite regions, (c) SEM micrograph of the cast alloy shows the γ–γ′ eutectic in the inter-dendrite region and (d) corresponding SEM-EDS of MC carbide.

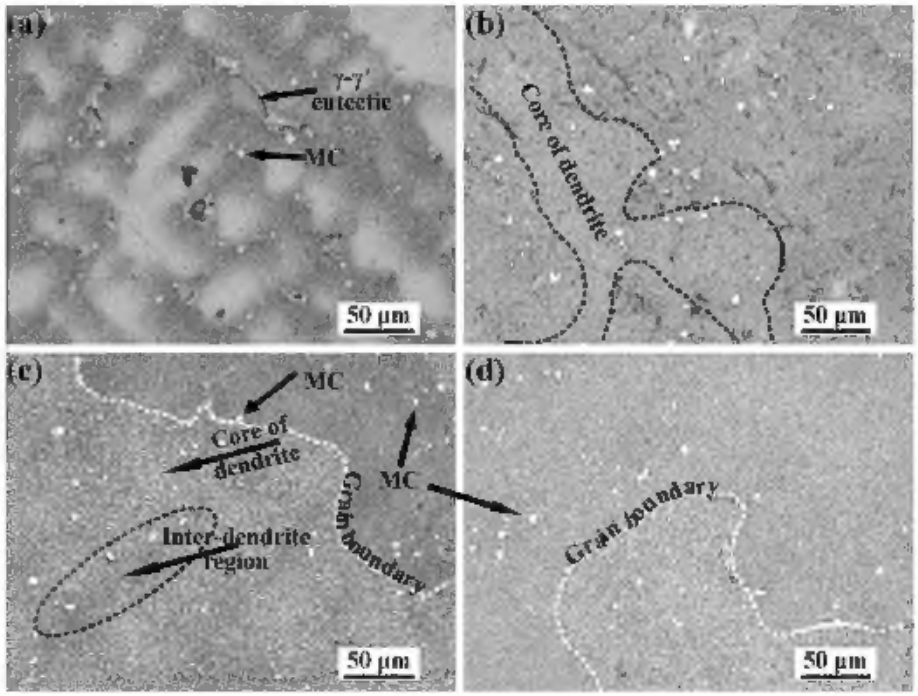

Fig. 3. The optical micrographs of the cast alloy and the alloys after each step of solution heat treatments, (a) cast alloy shows the distribution of the γ–γ′ eutectic and the MC carbide, microstructures after solution heat treatment at (b) 1204 °C/2 h AC (c) 1093 °C/4 h AC (d) 1054 °C/4 h AC.

Fig. 3 shows the optical micrographs of the cast alloy and the alloys after each step of solution heat treatments at 1204 °C/2 h AC + 1093 °C/4 h AC + 1054 °C/4 h AC. The γ–γ′ eutectic with "sector" morphology is found in the inter-dendrite region and MC carbide mainly precipitates in the inter-dendrite region (Fig. 3a). The enlarged γ–γ′ eutectic is shown in Fig. 2c. After solution heat treatment at 1204 °C for 2 h and AC, the γ–γ′ eutectic disappears and the dendrite segregation patterns can be identified in Fig. 3b. After following solution heat treatment at 1093 °C for 4 h and AC, the dendrite segregation patterns become vague, but they can be still identified in Fig. 3c. It is very hard to distinguish the dendrite segregation patterns after the third step of solution heat treatment shown in Fig. 3d. The MC carbide mainly precipitates in the inter-dendrite region of the cast alloy, however, some MC particles

are also found at the grain boundaries during the solution heat treatment (Fig. 3c). The γ–γ′ eutectic which results from the last stages of solidification has a lower melting point, and the γ–γ′ eutectic must be prevented in order to maintain the high temperature strength. The above results indicate that the γ–γ′ eutectic can be completely eliminated after solution heat treated at 1204 °C for 2 h and AC. Safari and Nategh [12] found that the γ–γ′ eutectic region is rich in Al and Ti elements, therefore, the average size of the γ′ particles in the inter-dendrite region is larger than that in the core of dendrite (Fig. 2c). The Ti has been known to be the MC carbide forming element in nickel-based superalloy and has a strong tendency to segregate in residual liquid during solidification [21]. Thus, as the solidification proceeds, the inter-dendritic liquid becomes a preferential site for MC carbide formation.

Fig. 4 shows SEM micrographs of the γ′ phase after each step of solution heat treatments at 1204 °C/2 h AC + 1093 °C/4 h AC + 1054 °C/4 h AC. Fig. 4a–c shows that the γ′ phase precipitates in the γ matrix with an approximately cubic shape. The volume fraction of the γ′ phase is measured according to the area fraction [7]. The average size of the γ′ phase is calculated according to the cube edge lengths and at least 200 γ′ particles are analyzed (Fig. 4d). The volume fraction and the average size of the γ′ phase are respectively about 23.3% and 371.5 nm after solution heat treated at 1204 °C/2 h AC (Fig. 4a). After solution heat treated at 1204 °C/2 h AC + 1093 °C/4 h AC, the volume fraction of the γ′ phase increases to about 27.6%, but the average size of the γ′ phase varies slightly (Fig. 4b). After full solution heat treatment, both the volume fraction and the average size of the γ′ phase further increase to about 33.8% and 458.9 nm (Fig. 4c), respectively.

Fig. 5 shows the morphology of the γ′ phase after aging treatment at 913 °C, 873 °C and 840 °C for 16 h, respectively. The γ′ phase shows a mixture of approximate spherical and cubic particles after aging treatments (Fig. 5a–c). The volume fraction and the average size of the γ′ phase are calculated (Fig. 5d). With the decrease of the aging temperature from 913 °C to 873 °C, the volume fraction slightly increases from about 37.1 to 42.7%, but the average size of the γ′ phase significantly decreases from about 411.2 nm to 383.6 nm (Fig. 5a and b). When the aging temperature further decreases to 840 °C, the volume fraction increases to about 45.6%, however, the average size of the γ′ phase further decreases to about 350.4 nm (Fig. 5c).

Fig. 6 shows the size distribution of the γ′ phase after the solution and aging heat treatments. The x value represents the average size of the γ′ particles. For example, $x = 200$ represents the γ′ particles with average size between 200 and 250 nm, $x = 250$ represents the γ′ particles with average size between 250 and 300 nm and so on. The y value data point or the height of the column represents the frequency of the γ′ particles with certain size. The peak columns shift to the right side (right side means that the γ′ particles are larger) significantly, which indicates that the average size of the γ′ phase increases after each step of solution heat treatments (Fig. 6a). However, Figs. 4d and 5d show that the average size of the alloys after aging heat treatments decreases compare with that after full solution heat treatments. Fig. 6b shows that the number of the γ′ particles with the size between 200 and 350 nm increases after aging heat treatment at 913 °C compare with that after solution heat treatment at 1054 °C. The γ′ particles with the average size between 200 and 350 nm increase significantly with the decrease of the aging temperature. The peak columns shift from $x = 400$ to $x = 350$ with the decrease of aging temperature. Besides, the frequency of γ′ particles with the average size between 200 and 250 nm increases dramatically after aging at 840 °C. Fig. 4c shows that very fine γ′ particles with the average size about 100 nm are identified among the coarse γ′ particles. The γ′ particles with the average size less than 200 nm are found in the aged samples in Fig. 5. So the above result indicates that parts of the fine γ′ particles can coexist with the coarse γ′ particles and grow up during the aging heat treatment. Hence, the average size of the γ′ particles after aging heat treatment decreases compare with that after solution heat treatment. Fig. 6b also shows that the frequency of the γ′ particles with the average size about 450–600 nm can be significantly reduced with the decrease of aging temperature, which indi-

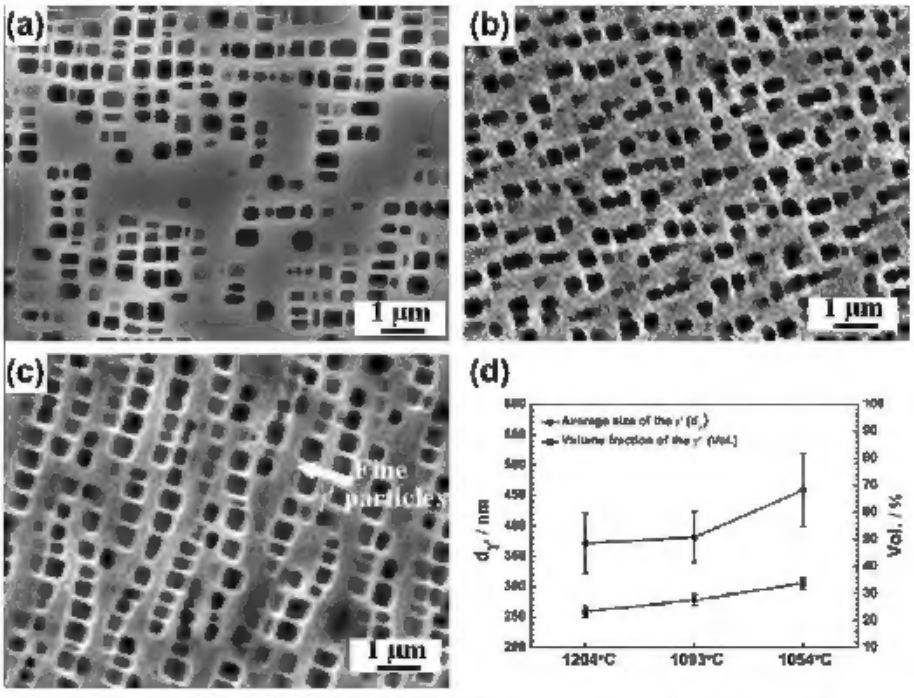

Fig. 4. SEM microstructures of the γ′ phase after solution heat treatment at (a) 1204 °C/2 h AC (b) 1093 °C/4 h AC (c) 1054 °C/4 h AC, and (d) shows the variation of the volume fraction and average size of the γ′ phase after each step of solution heat treatments.

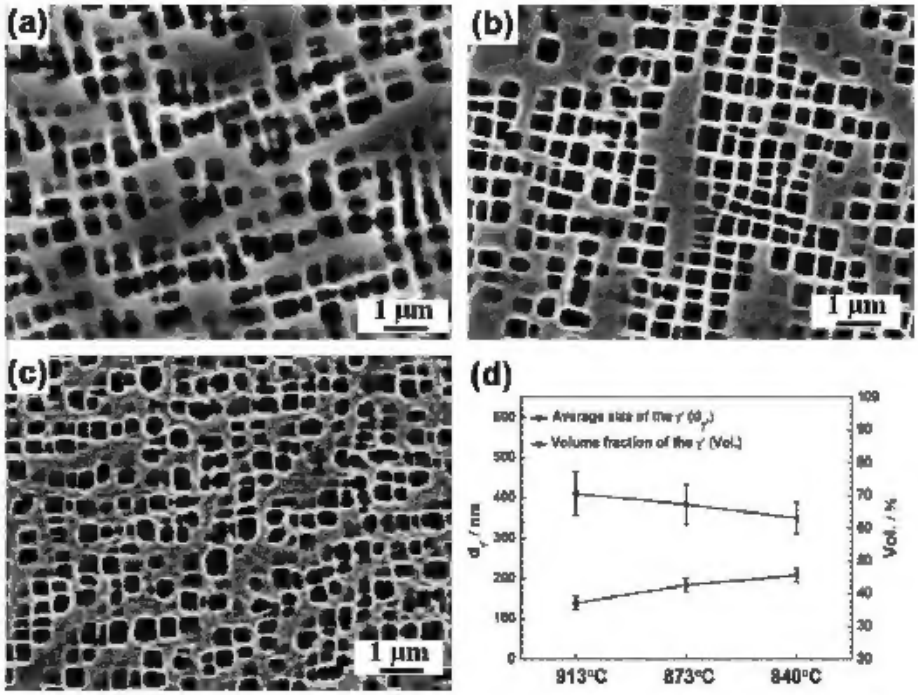

Fig. 5. SEM microstructures of the γ′ phase after aging heat treatment at (a) 913 °C/16 h AC, (b) 873 °C/16 h AC, (c) 840 °C/16 h AC, and (d) shows the variation of the volume fraction and average size of the γ′ phase after aging heat treatments.

cates that the lower aging temperature can suppress the growing of the coarse γ′ particles, but facilitate the growth of the fine γ′ particles.

Varying precipitate sizes resulted in different slip modes and different rates of fatigue crack propagation. It was found that small γ′ particles resulted in greatly reduced fatigue crack propagation rates in Waspaloy (Ni–19.2Cr–1.3Al–3.0Ti–13.9Co–0.05C–1.2Fe) [22]. Sajjadi et al. [23] reported that a high density of dislocations form around the γ′ particles during deformation at 650 °C of GTD-111 alloy with similar chemical compositions to Rene 80. The γ′ phase which retains its high degree of order up to the melting point has a cube-on-cube orientation relationship with the γ matrix and hinders dislocation motion [24,25]. The small sizes of the γ′ phase usually promote dislocation shearing while larger particles usually promote Orowan looping mechanism [22,26]. So the dislocation in the matrix would either slip away or would not penetrate through the γ′ phase when the size of the γ′ phase was large. Xu et al. [8] reported that the volume fraction of the γ′ phase had a significant effect on the mechanical properties of nickel-based superalloy. As a result, the increased volume fraction of the γ′ phase improves the mechanical properties of Rene 80 (Table 1).

Blocky MC carbide is identified at the grain boundaries and in the grain interior after each solution heat treatment and the typical SEM morphology is shown in Fig. 7. The corresponding SEM-EDS shows that the MC carbide is rich in Ti, W and Mo elements. The volume fraction of the MC carbide is about 3.1%. The morphology and the chemical composition after solution heat treatment change slightly compare with those in the casting ingot shown in Fig. 2c.

The microstructures of the γ′ phase and carbides in the alloys after aging heat treatment at 913 °C/16 h AC are shown in Fig. 8. In addition to the large MC carbide, very fine MC carbide is found precipitating along grain boundaries (Fig. 8a). The fine MC carbide with average width about 2 μm can be clearly seen from the enlarged morphology shown in Fig. 8b. Fig. 8b also shows that borides with "script" morphology are identified at the grain boundaries and the corresponding SEM-EDS reveals that the borides are rich in Mo, W and Cr elements. The γ′ phase with approximately cubic shape can also precipitate at regions near the grain boundaries.

After aging at 873 °C for 16 h AC, the precipitates of γ′ phase and carbides are shown in Fig. 9. Fig. 9a shows that script carbide is identified at the grain boundaries and the corresponding SEM-EDS shows that the carbide is M_6C which is rich in W, Ni, Co and Cr elements. Blocky MC carbide is also identified at the grain boundaries or in the grain interior and the size is nearly the same to that after solution heat treatments. Fig. 9b shows that $M_{23}C_6$ carbide is found near the MC carbide and the morphology is similar to that of the M_6C carbide. The corresponding SEM-EDS indicates that the $M_{23}C_6$ carbide is rich in Cr element. Hence, the chemical compositions of these carbides are significantly different and the above results are in accord with the previous research [12–14,27].

After aging at 840 °C for 16 h AC, the blocky MC and script $M_{23}C_6$ carbides are identified at grain boundaries in Fig. 10. The corresponding SEM-EDS indicates that the chemical compositions show very slight difference compare with those after aging at higher temperatures. The above results also show that MC carbide is rich in Ti, Mo and W elements. The MC carbide is found at the grain boundaries or in the grain interior after each step of heat treatments indicating that the MC carbide is the most stable carbide among the carbides and Ti in Rene 80 can stabilize the MC carbide. The presence of refractory metal elements such as W leads to the precipitate of M_6C carbide. After aging for a long time, the carbides have enough time to provide the carbon diffusion and react to form M_6C and $M_{23}C_6$ carbides. The M_6C and $M_{23}C_6$ have similar morphologies shown in Fig. 9. The M_6C carbide has a complex cubic structure and forms at slightly higher temperatures (815–980 °C) than that of $M_{23}C_6$ [12]. Figs. 8–10 show that the γ′ particles also precipitate near the carbides at the region near the grain boundaries after aging heat treatment at 913, 873 and 840 °C for 16 h. Choi et al. [27] also found that the growth of M_6C and $M_{23}C_6$ carbides at the grain boundary makes the alloy locally enrich of Al and Ti when the MC decomposes into M_6C and $M_{23}C_6$, which allows the γ′ particles to form along the grain boundary. The follow-

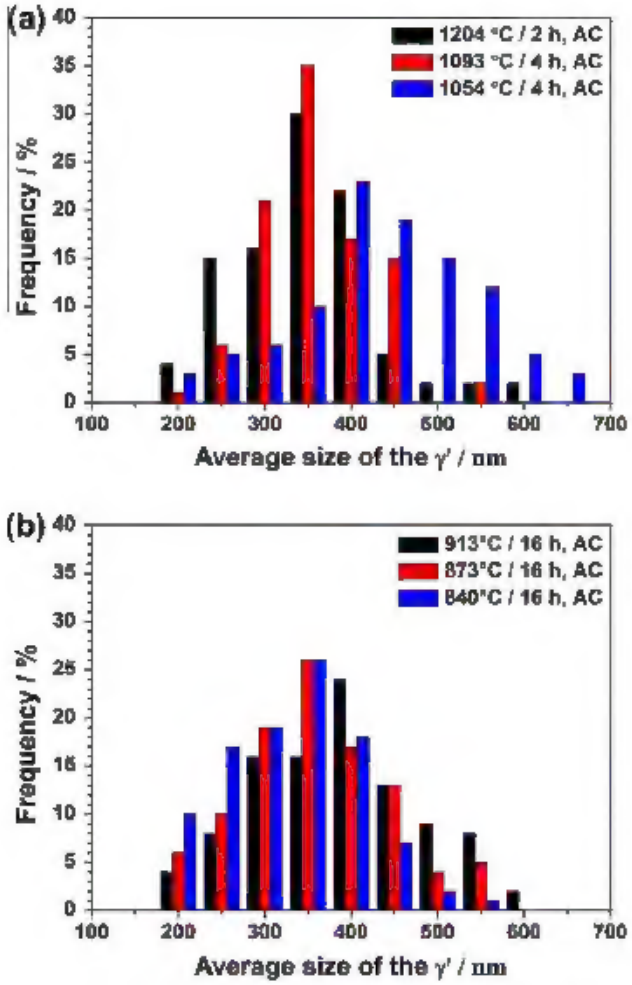

Fig. 6. Shows the size distribution of the γ′ phase after the (a) solution and (b) aging heat treatments.

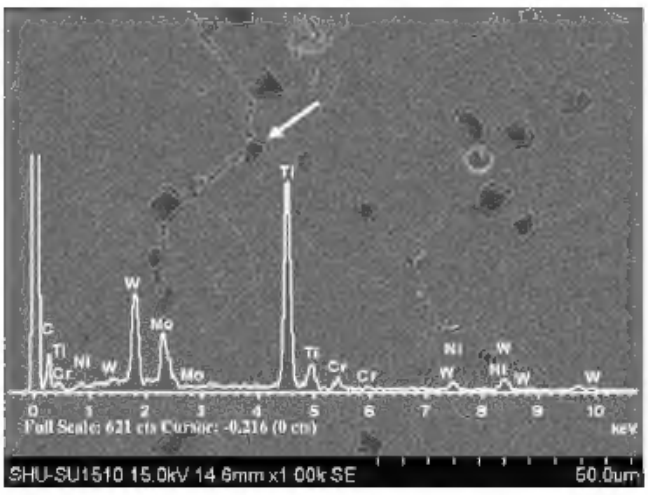

Fig. 7. The typical SEM morphology of the blocky MC carbide at the grain boundaries and in the grain interior after solution heat treatment.

ing reaction may lead to the formation of M_6C or $M_{23}C_6$ carbides at the grain boundaries during aging heat treatment [28]:

$$MC + \gamma \rightarrow M_6C \text{ or } M_{23}C_6 + \gamma'$$

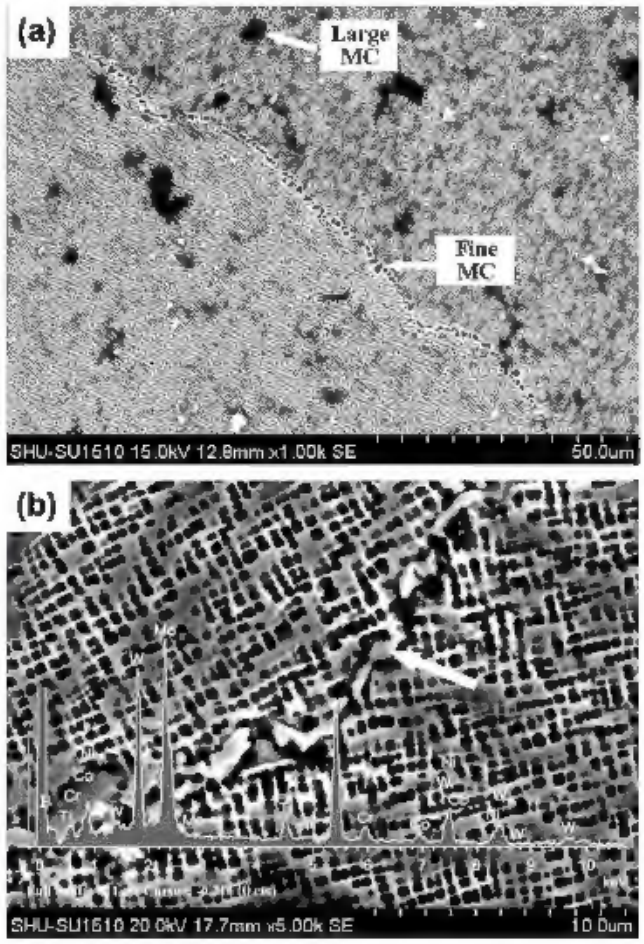

Fig. 8. The (a) microstructures of the γ′ phase and carbides in the alloys after aging heat treatment at 913 °C/16 h AC and (b) enlarged morphology and the corresponding SEM-EDS of the borides at the grain boundaries.

During the high temperature creep tests of cast nickel-based superalloy M963, the primary MC is found to decompose into M_6C continuously and Cr rich $M_{23}C_6$ carbide at the grain boundaries [29]. Carbide containing nickel-bases superalloys have superior high temperature mechanical properties compare with those strengthened only by the γ′ phase. The presence of discrete carbides along the grain boundaries can prevent the grain boundary sliding [28]. The $M_{23}C_6$ carbide precipitates at the grain boundaries enveloped within layers of γ′ phase is the ideal morphology for inhibiting grain boundary sliding and improving creep resistance [30]. So the borides with "script" morphology can precipitate at the grain boundaries at aging temperature about 913 °C, the M_6C carbide can precipitate at aging temperature about 873 °C, while the $M_{23}C_6$ carbide can precipitate at the grain boundaries at aging temperature 840–873 °C. The carbides mainly consist of block MC and a small amount of M_6C and $M_{23}C_6$ in Rene 80. The precipitate of carbides prevents the dislocation moving and grain boundary sliding, which can improve the mechanical properties of Rene 80.

As discussed above, with the decrease of aging temperature, the average size of the γ′ particles decreases, but the volume fraction of the γ′ particles increases. The lower aging temperature can suppress the growing of the coarse γ′ particles, but facilitate the growth of the fine γ′ particles. After the optimum heat treatment of 1204 °C/2 h AC + 1093 °C/4 h AC + 1054 °C/4 h AC + 840 °C/16 h AC, the ultimate tensile strength and yield strength are respectively higher than 1040 MPa and 950 MPa, the stress-rupture life at 871 °C/310 MPa is higher than 170 h with excellent ductility. The improved tensile strength at room temperature and stress-

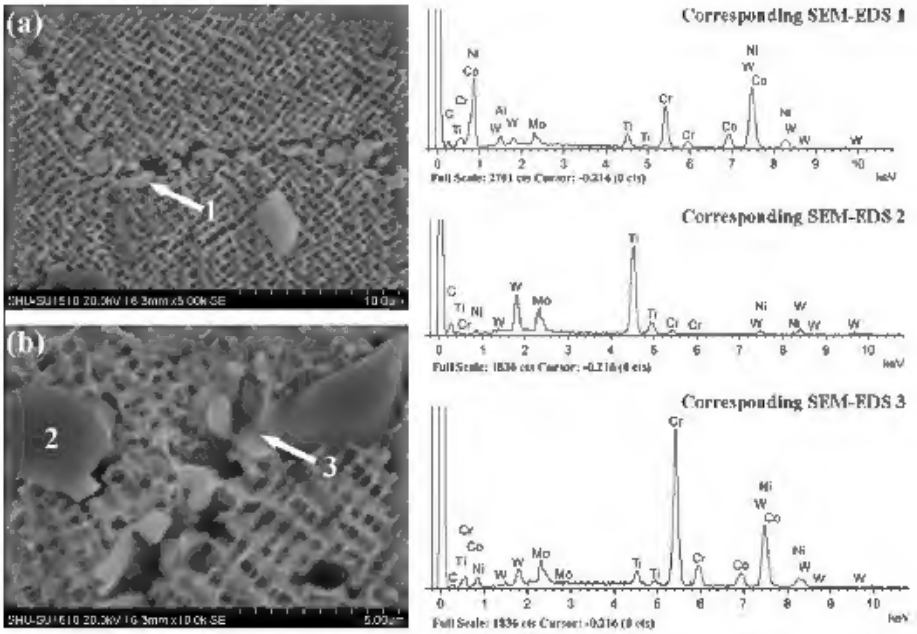

Fig. 9. The (a) morphology of γ′ phase and carbides after aging at 873 °C for 16 h AC and (b) enlarged morphology shows the M_6C, MC and $M_{23}C_6$ carbides.

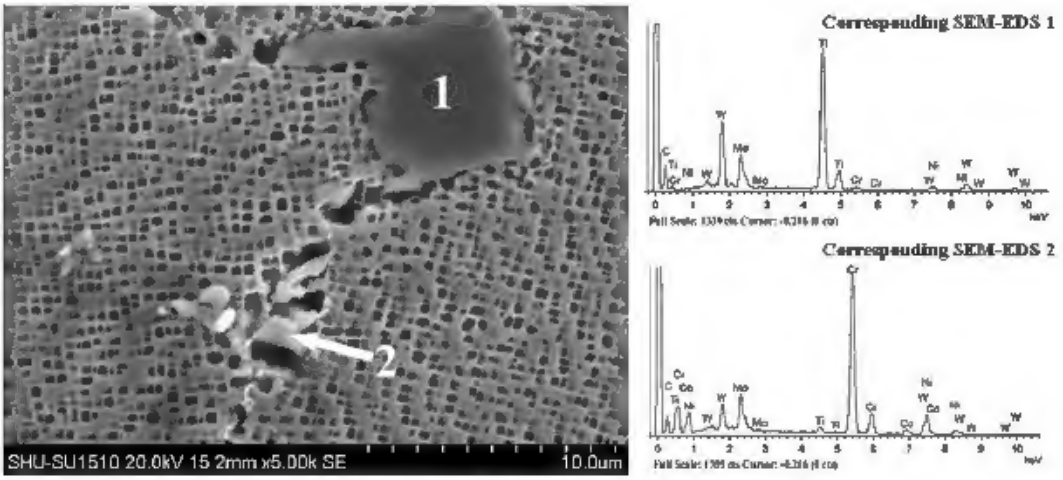

Fig. 10. The morphology of the blocky MC and script $M_{23}C_6$ carbides at grain boundaries after aging at 840 °C for 16 h AC.

rupture life at high temperature are primarily due to the increased volume fraction of the γ′ phase. And the precipitate of carbides at the grain boundaries may partly contribute to the improved mechanical properties of Rene 80.

4. Conclusions

Effects of heat treatments on room temperature mechanical properties and stress-rupture properties of Rene 80 nickel-based superalloy have been investigated. The following conclusions can be drawn:

(1) With the decrease of aging temperature, the average size of the γ′ phase decreases, but the volume fraction of the γ′ phase increases.
(2) The lower aging temperature can suppress the growth of the coarse γ′ particles, but facilitate the growth of the fine γ′ particles.
(3) After the optimum heat treatment of 1204 °C/2 h AC + 1093 °C/4 h AC + 1054 °C/4 h AC + 840 °C/16 h AC, the ultimate tensile strength and yield strength are respectively higher than 1040 MPa and 950 MPa, the stress-rupture life at 871 °C/310 MPa is higher than 170 h with excellent high temperature ductility. The improved tensile strength at room temperature and stress-rupture life at high temperature are primarily due to the increased volume fraction of the γ′ phase.
(4) The borides can precipitate at the grain boundaries at about 913 °C. The primary MC is found to decompose into M_6C at aging temperature about 873 °C and Cr rich $M_{23}C_6$ carbides at aging temperature 840–873 °C at the grain boundaries. The precipitate of the carbides may partly contribute to the improved mechanical properties.

Acknowledgments

The authors would like to thank Y.L. Chu for SEM analysis in Instrumental Analysis & Research Center of Shanghai University. This research was sponsored by Shanghai Leading Academic Discipline Project, Project Number: S30107.

References

[1] Tiley J, Viswanathan GB, Hwang JY, Shiveley A, Banerjee R. Evaluation of gamma prime volume fractions and lattice misfits in a nickel base superalloy using the external standard X-ray diffraction method. Mater Sci Eng A 2010;528:32–6.

[2] Goswami T, Hänninen H. Dwell effects on high temperature fatigue behavior – Part I. Mater Des 2001;22:199–215.

[3] Goswami T, Hänninen H. Dwell effects on high temperature fatigue damage mechanisms – Part II. Mater Des 2001;22:217–36.

[4] Sidhu RK, Ojo OA, Chaturvedi MC. Sub-solidus melting of directionally solidified Rene 80 superalloy during solution heat treatment. J Mater Sci 2008;43:3612–7.

[5] Collier JP, Wong SH, Tien JK, Phillips JC. The effect of varying Al, Ti and Nb content on the phase stability of Inconel 718. Metall Mater Trans A 1988;19:1657–66.

[6] Xu Y, Jin Q, Xiao X, Cao X, Jia G, Zhu Y, et al. Strengthening mechanisms of carbon in modified nickel-based superalloy Nimonic 80 A. Mater Sci Eng A 2011;528:4600–7.

[7] Xu Y, Yang C, Xiao X, Cao X, Jia G, Shen Z. Strengthening behavior of Al and Ti elements at room temperature and high temperature in modified Nimonic 80 A. Mater Chem Phys 2012;134:706–15.

[8] Xu Y, Yang C, Xiao X, Cao X, Jia G, Shen Z. Evolution of microstructure and mechanical properties of Ti modified superalloy Nimonic80 A. Mater Sci Eng A 2011;530:315–6.

[9] Aghaie-Khafri M, Hajjavady M. The effect of thermal exposure on the properties of a Ni-base superalloy. Mater Sci Eng A 2008;487:388–93.

[10] Pyczak F, Neumeier S, Göken M. Influence of lattice misfit on the internal stress and strain states before and after creep investigated in nickel-base superalloys containing rhenium and ruthenium. Mater Sci Eng A 2009;510–511:295–300.

[11] Wei CN, Bor HY, Chang L. The effects of carbon content on the microstructure and elevated temperature tensile strength of a nickel-base superalloy. Mater Sci Eng A 2010;527:3741–7.

[12] Safari J, Nategh S. On the heat treatment of Rene-80 nickel-base superalloy. J Mater Process Technol 2006;176:240–50.

[13] Sun WR, Lee JH, Seo SM, Choe SJ, Hu ZQ. The eutectic characteristic of MC-type carbide precipitation in a DS nickel-base superalloy. Mater Sci Eng A 1999;271:143–9.

[14] Wei CN, Bor HY, Chang L. The influence of carbon addition on carbide characteristics and mechanical properties of CM-681LC superalloy using fine-grain process. J Alloys Compd 2011;509:5708–14.

[15] Österle W, Krause S, Moelders T, Neidel A, Oder G, Völker J. Influence of heat treatment on microstructure and hot crack susceptibility of laser-drilled turbine blades made from Rene 80. Mater Character 2008;59:1564–71.

[16] Safari J, Nategh S. Microstructure evolution and its influence on deformation mechanisms during high temperature creep of a nickel base superalloy. Mater Sci Eng A 2009;499:445–53.

[17] Rahmani K, Nategh S. Isothermal LCF behavior in aluminide diffusion coated Rene 80 near the DBTT. Mater Des 2009;30:1183–92.

[18] Rahmani K, Nategh S. Influence of aluminide diffusion coating on the tensile properties of the Ni-base superalloy Rene 80. Surf Coat Technol 2008;202:1385–91.

[19] GB/T 228–2002. Metallic materials-tensile testing at ambient temperature. China Standard Press; 2002.

[20] GB/T 2039–1997. Metallic materials-creep and stress-rupture test in tension. China Standard Press; 1997.

[21] Liu LR, Jin T, Zhao NR, Wang ZH, Sun XF, Guan HR, et al. Effect of carbon additions on the microstructure in a Ni-base single crystal superalloy. Mater Letters 2004;58:2290–4.

[22] Lerch BA, Jayaraman N, Antolovich SD. A study of fatigue damage mechanisms in Waspaloy from 25 °C to 800 °C. Mater Sci Eng 1984;66:151–66.

[23] Sajjadi SA, Nategh S, Isac M, Zebarjad SM. Tensile deformation mechanisms at different temperatures in the Ni-base superalloy GTD-111. J Mater Process Technol 2004;155–156:1900–4.

[24] Coakley J, Basoalto H, Dye D. Coarsening of a multimodal nickel-base superalloy. Acta Mater 2010;58:4019–28.

[25] Divinski SV, Frank ST, Södervall U, Herzig CHR. Solute diffusion of Al-substituting elements in Ni_3Al and the diffusion mechanism of the minority component. Acta Mater 1998;46:4369–80.

[26] Sharma KK, Banerjee D, Tewari SN. Effect of reverse-aging treatment on the microstructure and mechanical properties of Nimonic alloys. Mater Sci Eng A 1988;104:131–40.

[27] Choi BG, Kim IS, Kim DH, Jo CY. Temperature dependence of MC decomposition behavior in Ni-base superalloy GTD 111. Mater Sci Eng A 2008;478:329–35.

[28] Garosshen TJ, Mccarthy GP. Low temperature carbide precipitation in a nickel base superalloy. Metall Trans A 1985;16:1213–23.

[29] He LZ, Zheng Q, Sun XF, Hou GC, Guan HR, Hu ZQ. $M_{23}C_6$ precipitation behavior in a Ni-base superalloy M963. J Mater Sci 2005;40:2959–64.

[30] Jena AK, Chaturvedi MC. The role of alloying elements in the design of nickel-base superalloys. J Mater Sci 1984;19:3132–9.